Soft Matter

Accepted Manuscript

ROYAL SOCIETY OF CHEMISTRY

www.rsc.org/softmatter

ARTICLE TYPE www. rsc.org/xxxxxx | XXXXXXXX

Scanning fluorescence correlation spectroscopy as a versatile tool to measure static and dynamic properties of soft matter systems †

Manish Nepal,[a] Alon Yaniv,[a] Oleg Krichevsky*[ab]

Received Xth XXXXXXXXXX 20XX, Accepted Xth XXXXXXXXX 20XX
First published on the web Xth XXXXXXXXXX 200X
DOI: 10.1039/b000000x

We present the formalism and experimental implementation of Scanning Fluorescence Correlation Spectroscopy (SFCS) for the measurements of soft matter system structure and dynamics. We relate the SFCS function Fourier transform to the system intermediate scattering function and demonstrate how SFCS can be combined with specific labelling to measure the desired statistical and kinetic features of the system. Using DNA as a model polymer, we demonstrate the application of SFCS to measure 1) the static structure factor of the system, 2) polymer end-to-end distance distribution, and 3) polymer segmental dynamics in dilute and in dense solutions. The measured DNA end-to-end distance distributions are close to Gaussian. Implementing SFCS we obtain reliable data on segmental mean-square displacement kinetics in dense solutions, where static FCS approach fails because of dye photobleaching. For moderate concentrations in semidilute regime (at ~ 7 overlap concentrations) segmental dynamics exhibit only weak entanglements. Both of these experimental findings are consistent with theoretical predictions of the weakness of excluded interactions in semiflexible polymers.

1 Introduction

Since its inception Fluorescence Correlation spectroscopy [1–4] (FCS) has been increasingly used to study the dynamics of fluorescent molecules (for reviews see [5–9]). The technique is based on collecting temporal correlation function of fluctuations in fluorescence emanating from a diffraction limited volume. Any kinetics in the system that is coupled to changes in fluorescence leaves its feature in the correlation function in the relevant time window. E.g. diffusion process results in emission fluctuations as fluorescent molecules move within/in/out of the sampling volume leading to the decay of the FCS correlation function in the time window of the characteristic diffusion times. But other kinetic features, such as fluorophore photodynamics, chemical reactions, intramolecular dynamics of DNA and proteins can also be assessed through appropriate labeling [10–15].

While in the standard implementation of FCS the correlation is done on the fluorescence signal arriving from the same location in the sample, several FCS modifications couple temporal and spatial information. In an early precursor to scanning FCS (SFCS), Weissmann et al [16,17] monitored fluorescence fluctuations in a moving sample: the quantity they measured is equivalent to the amplitude of the FCS correlation function, and this alone already allowed them to measure DNA lengths in their samples [16,17]. Similar information is obtained with Image Correlation Spectroscopy [18] (ICS) which can assess the sizes of molecular aggregates, their number densities and dynamics [19]. While later versions of ICS also analysed some features of spatiotemporal dynamics, the instrumental constraints limit such measurements to systems with very slow kinetics in the seconds range [20,21].

Scanning FCS has been employed mainly to improve on static FCS in measuring temporal dynamics [22–28]: typically, the sample or the beam moves in small circles fast enough so that any point on the trajectory is crossed repeatedly *within* the typical diffusion time. The resulting oscillations in the correlation function can be analysed to obtain diffusion coefficients of fluorescent molecules [29,30].

Recently, we have developed a different version of SFCS where small curvature trajectories approximate the constant velocity motion along a straight line. In our implementation, the beam only rarely passes through the same location [31,32]. We have shown that the structure factor of the system can be extracted from the FCS correlation functions collected in such fast scans.

In this paper, we present a detailed formalism for this technical approach and then take it further: we derive the relation between the intermediate scattering function of the labeled part of the system and SFCS measurements. Then using the example of DNA end-to-end distance distribution, we show how SFCS can be combined with specific labelling to measure some fine structural features of the sample. Furthermore,

[a] *Physics Department, Ben-Gurion University of the Negev, Beer-Sheva 84105, Israel. Fax: +97286472904; Tel: +97286472123; E-mail: okrichev@bgu.ac.il*
[b] *Ilse Kats Centre for Nanoscience, Ben-Gurion University, Beer-Sheva 84105, Israel.*

we show that dense systems with complex dynamics extending over a wide range of time scales can be studied with SFCS performed at multiple speeds. In such systems, a significant part of the dynamics is often slow and the conventional FCS approach gives erroneous results even at short time scales because of the photobleaching.

We begin by deriving the formalism for our implementation of SCFC. Then we describe our experimental design, calibrations, analysis and sample preparation methods. Finally, we demonstrate application examples of SFCS to characterize DNA end-to-end distance distributions in dilute solutions and to measure DNA segmental dynamics in dense solutions.

2 Theoretical Background

In this section we first derive the general formalism of our implementation of SFCS, and then we apply it to several particular cases of interest for experiments.

2.1 General SFCS formalism

We start by generalising the well established FCS formalism[3,33] for the situation of structured fluorescence objects (not necessarily point-like) with complex dynamics and with added sample scanning. We assume that in the statistical sense the sample is spatially homogeneous and denote the spatiotemporal distribution of fluorescent molecules by their local concentration field $c(\mathbf{r},t)$. The spatial intensity distribution of excitation beam and detection efficiency is characterised by the optical transfer function (OTF) of the setup $I(\mathbf{r})$. We will further assume that the emission response is linear in excitation intensity and write the instantaneous $I_{\mathrm{em}}(t)$ and average $\langle I_{\mathrm{em}}\rangle$ collected emission and its fluctuations $\delta I_{\mathrm{em}}(t) = I_{\mathrm{em}}(t) - \langle I_{\mathrm{em}}\rangle$ respectively as:

$$I_{\mathrm{em}}(t) = Q\int c(\mathbf{r},t)I(\mathbf{r})d\mathbf{r}, \tag{1}$$

$$\langle I_{\mathrm{em}}\rangle = Q\bar{c}\int I(\mathbf{r})d\mathbf{r}, \tag{2}$$

$$\delta I_{\mathrm{em}}(t) = Q\int \delta c(\mathbf{r},t)I(\mathbf{r})d\mathbf{r}, \tag{3}$$

where $\delta c(\mathbf{r},t) = c(\mathbf{r},t) - \bar{c}$ are the concentration fluctuations while $\bar{c}$ is the average concentration and Q represents the fluorophore brightness and photon collecting efficiency of the setup.

We define the temporal autocorrelation function of emission fluctuations for a time lag t as:

$$G(t) = \langle \delta I_{\mathrm{em}}(0)\delta I_{\mathrm{em}}(t)\rangle / \langle I_{\mathrm{em}}\rangle. \tag{4}$$

Using Eqs. 1-4, we have:

$$G = \frac{Q}{\bar{c}\int I(\mathbf{r})d\mathbf{r}}\int d\mathbf{r}d\mathbf{r}' I(\mathbf{r})I(\mathbf{r}')\langle \delta c(\mathbf{r},0)\delta c(\mathbf{r}',t)\rangle \tag{5}$$

Note that our normalisation in the Eq. 4 is different from the standard FCS definition which has $\langle I_{\mathrm{em}}\rangle^2$ in the denominator instead of $\langle I_{\mathrm{em}}\rangle$. In our context the definition by the Eq. 4 happens to be more convenient since for Poisson statistics $\langle \delta c(\mathbf{r},0)\delta c(\mathbf{r}',0)\rangle = \bar{c}\delta(\mathbf{r}'-\mathbf{r})$ and therefore G in the Eq. 5 does not depend explicitly on the fluorophore concentration.

Assume now that in the course of FCS measurement the sample is scanned with a constant velocity $\mathbf{V}$ and let the coordinate system move with the sample. Eq. 5 becomes:

$$G = \frac{Q}{\int I(\mathbf{r})d\mathbf{r}}\int d\mathbf{r}d\mathbf{r}' I(\mathbf{r})I(\mathbf{r}'+\mathbf{V}t)g(\mathbf{r}'-\mathbf{r},t), \tag{6}$$

where $g(\mathbf{r},t) = \langle \delta c(\mathbf{0},0)\delta c(\mathbf{r},t)\rangle/\bar{c}$ is the van Hove density-density time-correlation function (up to an additive constant of $\bar{c}$). Then switching to Fourier domain we can write :

$$G(\mathbf{R},t) = \frac{Q(2\pi)^3}{\int I(\mathbf{r})d\mathbf{r}}\int d\mathbf{q}|I(\mathbf{q})|^2 F(\mathbf{q},t)e^{i\mathbf{qR}} \tag{7}$$

where $F(\mathbf{q},t) = \frac{1}{N}\langle \delta c^*(\mathbf{q},0)\delta c(\mathbf{q},t)\rangle$ is the so-called intermediate scattering function[34] with N being the total number of fluorescent molecules in the sample, $\mathbf{R} = \mathbf{V}t$ is the sample displacement within time t, and $I(\mathbf{q})$ is the mode transfer function (MTF) of the setup. This result differs from the standard static FCS expression[33,35] by a phase factor $e^{i\mathbf{qR}}$.

We find it instructive to look at Eq. 7 the following way: suppose the measurement is performed with a large set of different speeds $\{\mathbf{V}_j\}$. Then G in Eq. 7 can be considered a function of two independent parameters $\mathbf{R}$ and t: for each t there will be made a large set of measurements with different $\mathbf{R}_j = \mathbf{V}_j t$. Then if $I(\mathbf{q})$ is calibrated, $F(\mathbf{q},t)$ can be obtained from Eq. 7 by spatial Fourier transform of $G(\mathbf{R},t)$ for each time point t. As far as we can see, this is the most general formulation for extracting spatial-temporal correlations from the scanning FCS data. The intermediate scattering function is usually measured by dynamics light scattering technique[33]. The potential advantage of SFCS measurements is their combination with specific fluorescence labelling so that the dynamics of only objects of interest is highlighted.

Since in practice the set of useful $\{\mathbf{R}_j\}$ is limited and sparse, it is difficult to apply the formalism in its most general form to the experimental data. Thus, we discuss below a few particular cases of the general approach assessing: 1) the static structure factor of the sample, 2) the end-to-end distance distribution of a polymer chain, and 3) the dynamics of a polymer segment in dense solutions. In each of these cases, some additional conditions can be set onto the intermediate scattering function that facilitate the analysis of the measurements. While these three situations are relevant to our experiments, the general approach can be applied to other cases where $F(\mathbf{q},t)$ dependence can be constrained by appropriate models (some examples of such models can be found in[36]).

2.2 Structure factor measurement with SFCS

If the sample is homogeneously labeled with fluorophores (e.g. DNA molecules or other polymers tagged along their contour) its structure factor can be measured by performing SFCS with a single velocity $\mathbf{V}$ so high that the dynamics of the system during the passage time through the confocal spot can be neglected. Indeed, in this case the explicit time dependence of $F(\mathbf{q},t)$ and $G(\mathbf{R},t)$ in Eq. 7 can be neglected in comparison to the implicit temporal dependence through $\mathbf{R} = \mathbf{V}t$. We can then set $t = 0$ in $F(\mathbf{q},t)$ and $G(\mathbf{R},t)$. For homogeneous labelling, $F(\mathbf{q},0)$ is by definition the sample structure factor $S(\mathbf{q})$. Then (skipping normalisation):

$$G(\mathbf{R}) \propto \int d\mathbf{q}|I(\mathbf{q})|^2 S(\mathbf{q}) e^{i\mathbf{qR}}, \tag{8}$$

which means that the Fourier transform of $G(\mathbf{R})$ is

$$G(\mathbf{q}) \propto S(\mathbf{q})|I(\mathbf{q})|^2 \tag{9}$$

The physical meaning of these expressions is rather simple: when the sample is scanned at high speed, the local concentration fluctuations are "frozen" in the course of the beam passage. Then the temporal correlations measured with FCS reflect the spatial correlations in the sample with $\mathbf{R} = \mathbf{V}t$ time to space conversion. More precisely, since our OTF is not point-like, the obtained correlation function is a convolution of the sample's spatial correlations with the system's OTF. As for any convolution then, one can deconvolve the two contributions in the Fourier space, obtaining a Fourier transform of the spatial correlations, i.e. the structure factor.

We would like to stress that the true solution structure factor is obtained when the sample is labeled homogeneously. This would be the same $S(\mathbf{q})$ that is measured by static light scattering (SLS). However, since fluorescent tags can be placed specifically, SFCS is much more versatile than SLS. E.g. only a small minority of chains can be labeled in a dense polymer solution and this way the polymer matrix effect onto the structure of individual chains can be studied. In this sense, SFCS is similar to neutron scattering measurements of deuterated synthetic polymers[37–39], but works at larger spatial scales comparable to visible light wavelength. This enhanced versatility and insensitivity to the presence of dust in the sample, makes SFCS very useful for measuring the properties of DNA solutions.

2.3 SFCS for end-to-end distance distribution measurements in DNA

Another useful application of specific fluorescent labelling is targeting particular locations within a molecule allowing to study the correlations *inside* the molecule. One of the examples of such approach that we consider here is the specific labelling of DNA polymer ends in combination with SFCS to study the end-to-end distance distributions. As in the preceding subsection, we will assume fast scanning, i.e. $F(\mathbf{q},t)$ can be replaced by $F(\mathbf{q},0)$. Assuming dilute solution of N DNA molecules tagged at their ends, we have $F(\mathbf{q},0) = \frac{1}{N}\langle|\delta c(\mathbf{q},0)|^2\rangle = 1 + \langle e^{i\mathbf{qr}_{12}}\rangle$, where $\mathbf{r}_{12} = \mathbf{r}_2 - \mathbf{r}_1$ is the instantaneous end-to-end distance in a DNA molecule and $\langle e^{i\mathbf{qr}_{12}}\rangle$ is the the characteristic function/Fourier transform $P_{ee}(\mathbf{q})$ of the end-to-end probability density function $P_{ee}(\mathbf{r}_{12})$.

Substituting this into Eq. 7, we have

$$G(\mathbf{R}) = G_1(\mathbf{R}) + G_{12}(\mathbf{R}), \tag{10}$$

where

$$G_1(\mathbf{R}) = \frac{Q}{\int I(\mathbf{r})\mathbf{r}} \int d\mathbf{q}|I(\mathbf{q})|^2 e^{i\mathbf{qR}} \tag{11}$$

stems from the self-correlation of a label with itself and therefore it can be measured independently by SFCS on single end labelled chains. The second term in Eq. 10:

$$G_{12}(\mathbf{R}) = \frac{Q}{\int I(\mathbf{r})\mathbf{r}} \int d\mathbf{q}|I(\mathbf{q})|^2 P_{ee}(\mathbf{q}) e^{i\mathbf{qR}} \tag{12}$$

reflects the cross-correlation in positions between the two ends of a DNA molecule that we are interested in. Notice that $G_{12}(\mathbf{R})$ is related to $P_{ee}(\mathbf{q})$ in the same manner that the $G(\mathbf{R})$ of a homogeneously labelled sample is related to $S(\mathbf{q})$ (Eq. 9):

$$G_{12}(\mathbf{q}) \propto P_{ee}(\mathbf{q})|I(\mathbf{q})|^2 \tag{13}$$

Thus we can measure $G(\mathbf{R})$ and $G_1(\mathbf{R})$ respectively on double- and single-end labeled solutions of DNA and determine $G_{12}(\mathbf{R})$ from their difference. The characteristic function $P_{ee}(\mathbf{q})$ can be further determined by performing Fourier transform on $G_{12}(\mathbf{R})$. Notice, that under the chosen normalisation $G(\mathbf{R})$ and $G_1(\mathbf{R})$ do not depend on concentration so there is no need in any adjustment of concentrations to perform the measurements.

We present the examples of using this approach in Subsection 4.1

2.4 Measuring dynamics in dense solutions using SFCS

Static FCS has been widely used to measure the molecular diffusion both *in vitro* and *in vivo*[5,7,8]. One of the limitations of this method is a case of very slow kinetics, when fluorophores photobleach before the molecule transit through the sampling volume. The photobleaching occurs mostly in the center of the illuminated field which increases the relative contribution of the field periphery. Altogether these distort the shape of the effective sampling volume, rendering FCS results intractable at all time scales. This is especially true for complex and dense environments where molecular kinetics might have subdiffusive character, i.e. being relatively fast at short time scales and slowing down at long time scales.

Here we show that scanning FCS can rescue the measurements by removing the molecules from the sampling volume before they photobleach. In this section we develop an appropriate formalism for dealing with such dense conditions. Results illustrating the use of this method to study the dynamics of DNA segments in semidilute solutions are presented in subsection 4.2

We keep the standard assumptions made in the derivation of static FCS formalism[3,40,41]. First, we assume similar independent sources of fluorescence, which gives $F(\mathbf{q},t) = \langle e^{i\mathbf{q}\Delta\mathbf{r}(t)}\rangle$ with $\Delta\mathbf{r}(t) = \mathbf{r}_j(t) - \mathbf{r}_j(0)$ being the fluorescence source j displacement over time t. Next, we assume that the molecular displacements $\Delta\mathbf{r}(t)$ are normally distributed. Then $F(\mathbf{q},t) = e^{-q^2\langle\Delta r^2(t)\rangle/6}$ holds with $\langle\Delta r^2(t)\rangle$ representing the mean square displacement (MSD) of a label at time t. Finally, we approximate the setup OTF by a Gaussian (see Subsection 3.3) and assume that $\mathbf{V}$ lies in the lateral plane. Under these assumptions, the Eq. 7 can be readily integrated leading to:

$$G = G_0(t)\exp\left[-\frac{(Vt)^2}{w_{xy}^2\left(1+\frac{2\langle\Delta r^2(t)\rangle}{3w_{xy}^2}\right)}\right], \qquad (14)$$

where G_0 is the FCS correlation function in static mode:

$$G_0 = \frac{Q}{2\sqrt{2}}\left(1+\frac{2\langle\Delta r^2(t)\rangle}{3w_{xy}^2}\right)^{-1}\left(1+\frac{2\langle\Delta r^2(t)\rangle}{3w_{xy}^2\omega^2}\right)^{-1/2}, \qquad (15)$$

where w_{xy} and ω define the effective dimensions of the sampling volume (see Subsection 3.3).

For the particular case of the diffusion of small molecules $\langle\Delta r^2(t)\rangle = 6Dt$ the Eqs. 14 & 15 give:

$$G = G_0(t)\exp\left[-\frac{(Vt)^2}{w_{xy}^2(1+t/\tau)}\right] \qquad (16)$$

with

$$G_0 = \frac{Q}{2\sqrt{2}}\left(1+\frac{t}{\tau}\right)^{-1}\left(1+\frac{t}{\tau\omega^2}\right)^{-1/2}, \qquad (17)$$

where $\tau = w_{xy}^2/(4D)$ as first derived by Magde et al[17] .

Eq. 14 can be used in the following way, alluded to above: the measurement is performed with a large set of different speeds $\{\mathbf{V}_j\}$ and for each time point G is considered as a function of $R_j = V_j t$. From Eq. 14 we expect this dependence to be Gaussian with the width related to molecular MSD at that time point. This allows us to extract $\langle\Delta r^2(t)\rangle$ dependence from such measurements.

3 Materials and Methods

In this section we discuss the experimental realisation of SFCS technique: the instrumentation, scan speed and OTF calibrations, correlation function Fourier analysis and sample preparation.

3.1 SFCS Instrumentation

Our experiments were carried out in a home built confocal SFCS setup. The fluorescence excitation was provided by the 514 nm line of an Ar-ion laser (Advantage 163D Spectra-Physics). The beam was expanded to ~ 4.5 mm underfilling the rear pupil of high power objective lens (~ 7.2 mm, UPLAPO 60X1.2W, Olympus). The beam power was kept in $2-10$ μW range before the objective. A dichroic mirror (Q525 Chroma) and a bandpass filter (HQ565/80, Chroma) were used to respectively deflect the laser line into the objective and to filter out extraneous light from the emission collected by the same lens. The emission light was focused onto a multimode optical fibre (50 μm core) that feeds it to a photon counting avalanche photodiode (SPCM-AQR-15-FC PerkinElmer). The photodiode pulses are correlated by a digital correlator (Flex2k-12Dx2, correlator.com). A flexure XY piezo-stage (Tritor 101,PiezoSystem Jena, or Nano-PDQ 275HS, Mad City Labs) with position sensors is used to scan the sample. The stage motion is controlled and its position monitored through by a DAQ board (National Instruments) Typically, 30 to 60 correlation functions are collected in short stretches of 10 s after the speed of scanning has settled on the desired value, and then averaged.

3.2 Stage motion

Strictly speaking the SFCS formalism outlined in Subsection 2.2 assumes a linear motion with a constant velocity. However, this requirement can be relaxed to a constant speed motion along any trajectory as long as its radius of curvature is much larger than other characteristic lengths in the system, such as the sampling volume size of (~ 0.25 μm) and solution correlation length ($< 1\mu$m in our experiments). In practice, the sample was scanned in the lateral plane along a trajectory of an imperfect circle of 52 μm (for Nano-PDQ) or 60 μm (for Tritor stage) diameter whose centre orbits along another circular trajectory of 30 μm (for Nano-PDQ) or 40μm (for Tritor stage) diameter. This pattern of scanning is chosen to cover a large surface area and to avoid frequent revisiting of the same positions, thereby diminishing photobleaching and correlated noise problems.

The piezo-stages were "trained" to perform constant speed motion to within 1-2 % (standard deviation). In general, piezo-stage motion has problems of nonlinearity, hysteresis and creep. However, for the same control input (i.e. DAQ output) pattern it is highly reproducible. Therefore the DAQ output pattern was modified and calibrated *prior* to the experiments until the appropriate speed stability was reached. Then

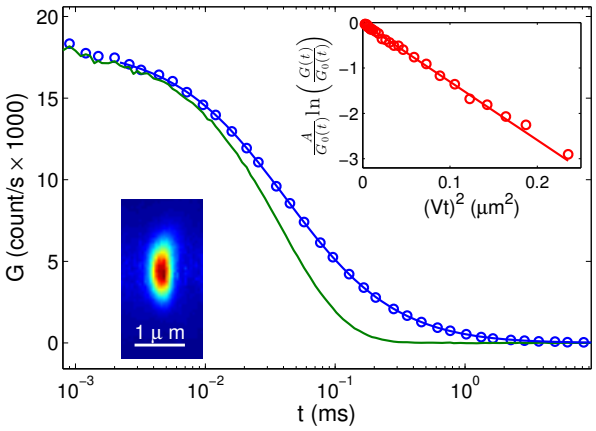

Fig. 1 OTF calibration: Static (blue circles) and scanning at 4400 $\mu m/s$ (green line) FCS measurements of freely diffusing Rh6G molecules. The blue line is fit to the static data with the Eq. 17 from which ω is determined. *Top inset* demonstrates the calibration of w_{xy}: circles represent the LHS of the Eq. 20 calculated from the FCS data in the figure, the blue line is a fit to the data with the RHS of the Eq. 20. *Bottom inset* shows direct imaging of OTF by scanning gold nano particles in X-Z plane

these output patterns were used during the experiment. The maximal speed reached was ~ 4 mm/s and the majority of the structural measurements were done at this speed. For the measurements of DNA dynamics in dense solutions we scan the sample at a set of speeds $\{V_j\}$ from low $\sim 1\mu m/s$ increasing with 10% step to $\sim 4400\ \mu m/s$. For each run the speed from the set is picked at random.

3.3 OTF calibration

For confocal setups with an underfilled rear objective pupil (as in our system) the OTF and, respectively, its MTF can be well approximated by an axisymmetric Gaussian functions:

$$I(\mathbf{r}) = I_0 \exp\left(-\frac{2(x^2+y^2)}{w_{xy}^2} - \frac{2z^2}{\omega^2 w_{xy}^2}\right), \quad (18)$$

$$I(\mathbf{q}) = I_0 \frac{\omega w_{xy}^3}{8} \exp\left(-\frac{w_{xy}^2}{8}(q_x^2+q_y^2) - \frac{\omega^2 w_{xy}^2}{8} q_z^2\right), \quad (19)$$

where $\omega = w_z/w_{xy}$, w_{xy} and w_z respectively define the aspect ratio and the radial and axial extent of the OTF.

Thus the two parameters, w_{xy} and ω fully define OTF and MTF of the setup. The aspect ratio ω can be determined from the fits with Eq. 17 to static FCS measurements of freely diffusing small molecules, such as fluorophores (Fig. 1) or short labeled dsDNA oligonucleotides. We do this calibration before each measurement and, typically, we obtain $\omega \approx 5.5 \pm 0.5$.

To determine w_{xy}, we notice that for short time scales, such that $\langle \Delta r^2(t) \rangle \ll \omega^2 w_{xy}^2$ in Eqs. 14 & 15 (or $t \ll \omega^2 \tau$ in Eqs. 16 & 17), the time dependence of $\ln(G_0/G)$ is similar to $G_0(t)$. So w_{xy} can be determined in the static and scanning FCS measurements performed on the same single labeled molecules from:

$$\frac{A}{G_0(t)} \ln\left(\frac{G(t)}{G_0(t)}\right) = -\frac{(Vt)^2}{w_{xy}^2}, \quad (20)$$

where $A = Q/2\sqrt{2} = G_0(t \to 0)$ is the amplitude of the static FCS correlation function G_0 that can be determined either by fitting static FCS correlation measurements with Eq 15 or by averaging the G_0 at short time scales $t \ll \tau$. The scanning speed V in this measurement should be high enough so that $G_0(t)$ and $G(t)$ dependences are sufficiently different from each other. Since $\omega^2 \approx 30 \gg 1$, the range of the applicability of the Eq. 20 (i.e. $t \ll \omega^2 \tau$) is rather wide.

In practice, we have been using Rh6G molecules, short labeled dsDNA oligonucleotides and even end-labeled long DNA molecules (of several thousands base pairs) for OTF calibrations giving identical results of $w_{xy} = 0.25 \pm 0.01 \mu m$. The amplitude A was typically determined by averaging data points in 1 to 2 μs range where G_0 plateaus ($\tau \approx 40\ \mu s$). Typical calibrations are shown in Fig 1.

We have also directly measured the OTF by confocal microscopy imaging of 50 nm gold beads. The resulting OTF is consistent with our SFCS/FCS calibrations (bottom inset in Fig. 1), but is too noisy to directly determine the MTF from the data. As a test for the effect of OTF deviations from the Eq. 18, we have fitted each of the lateral line profiles with a Gaussian: the fits are all very good but have slightly different widths, therefore deviating somewhat from the Eq. 18. Up to $q \sim 20\ \mu m^{-1}$ the analysis of SFCS data using such calibration gave results identical to those obtained assuming the OTF shape of Eq. 18.

3.4 Fourier Transform of the Correlation Function

In moving from the Eq. 8 to the Eq. 9, one needs to find $G(\mathbf{q})$ from $G(\mathbf{R})$. Strictly speaking this requires SFCS scans with constant velocity along each possible direction. However, for spatially homogeneous, isotropic sample there is enough information in the lateral scans alone (as mentioned in Subsection 3.2) in order to obtain the necessary Fourier transforms.

Indeed, let's split $\mathbf{R}$ and $\mathbf{q}$ into their lateral $\mathbf{R}_\perp$ and $\mathbf{q}_\perp$ and axial Z and q_z components respectively. Then from the Eq. 8:

$$G(\mathbf{R}_\perp, Z) \propto \int d\mathbf{q}_\perp dq_z |I(\mathbf{q}_\perp, q_z)|^2 S(q) e^{i\mathbf{q}_\perp \mathbf{R}_\perp + iq_z Z}, \quad (21)$$

where S is solely the function of $q = \sqrt{\mathbf{q}_\perp^2 + q_z^2}$ for an isotropic sample. Since we do only lateral scans, in our case $Z = 0$ and the correlation function we measure is $G(R_\perp, 0)$ with $R_\perp = Vt$

where we skip vector notations since $G(\mathbf{R}_\perp,0)$ is an isotropic 2D function.

Then lateral Fourier transform $G(\mathbf{q}_\perp,0)$ of $G(\mathbf{R}_\perp,0)$ is readily obtained by the Fourier-Bessel/Hankel transform (2D Fourier transform for isotropic functions) of the measured correlation functions. It is clear from the Eq. 21 that $G(\mathbf{q}_\perp,0)$ is related to the MTF calibration $I(\mathbf{q})$ and to $S(q)$ through:

$$G(q_\perp,0) \propto \int dq_z |I(q_\perp,q_z)|^2 S(q). \qquad (22)$$

Therefore the problem is reduced to that of finding $S(q)$ from the Eq. 22 with known MTF and $G(q_\perp,0)$. We do this in an iterative procedure, exploiting a weak dependence of OTF in axial direction (since $\omega^2 >> 1$). As a first step in the iteration we assume no axial dependence of the OTF, i.e. $\omega^2 \to \infty$, resulting in $I(q_\perp,q_z) = I(q_\perp)\delta(q_z)$. Then from Eqs. 22 and 19 the first approximation for the structure factor is given by $S^{(1)}(q_\perp) \propto G(q_\perp,0)\exp(w_{xy}^2 q_\perp^2/4)$.

We then calculate the expected $G^{(1)}(q_\perp,0)$ from Eq. 22 with the full $I(q_\perp,q_z)$ of the Eq. 19 and with the obtained $S^{(1)}(q)$. The difference $\delta G^{(1)}(q_\perp,0) = G(q_\perp,0) - G^{(1)}(q_\perp,0)$ between the measured and expected functions is used to calculate the next order correction for S(q) that is done again by assuming $\omega^2 \to \infty$: $\delta S^{(1)}(q_\perp) \propto \delta G^{(1)}(q_\perp,0)\exp(w_{xy}^2 q_\perp^2/4)$. This leads to the improved approximation for the structure factor: $S^{(2)}(q) = S^{(1)}(q) + \delta S^{(1)}(q)$. Now the next approximation $G^{(2)}(q_\perp,0)$ can be calculated from Eq. 22 using $S^{(2)}(q)$ and the iteration process can be repeated any number of times. However due to the high accuracy of the initial approximation, one step iteration is usually sufficient for the convergence.

We apply the same procedure to G_{12} (Eq. 14) in order to extract the characteristic function $P_{ee}(q)$ of the end-to-end distance distribution.

3.5 Sample preparation

In this work we study long DNA chains whose ends (either single or both) are selectively labeled with fluorescent dyes (Rh6G). We adapted various molecular biology techniques in order to create such DNA chains whose end regions have fluorescent dyes. Our approach can be summarised briefly as follows: we first create small DNA fragments with covalently attached fluorescent dye and then we ligate such fragments to long DNA ends.

In our approach of labeling ends of long DNA chains, we first amplify small DNA fragment with an analog nucleotide amino-allyl-dUTP (AA-dUTP) substituted for native nucleotide (dTTP) in the ratio of 1:1 by polymerase chain reaction (PCR). We amplify about 210bp region of pUC19 plasmid with primer sets 5'-GTCGACTCTAGAGGATCCCCG-3' (Forward) and 5'-CACGACAGGTTTCCCGACTGG-3'(Reverse).The forward primer has several restriction sites for ligation to longer DNA with the matching restriction site. For PCR reaction we obtained consistent and reliable result with 50 μL reaction volume and the final concentrations of reaction mixture as follows: 400 μM dNPTs, 5 mM Mg++, 5 μM primers, 5 ng template and 0.5 μL Taq polymerase solution (New England Biolabs). Thermal cycling was done for 35 cycles under the following conditions: denaturation at 98 C for 10 s, annealing for 30 s at 3 C above the lower annealing temperature recommended by the primer manufacturer (Midland Certified) and extension time was 2 min at 72 C. Following PCR we cleaned the reaction mixture using the commercially available clean-up kit (GE Healthcare) following the recommendations of the manufacturer. We then reacted the PCR amplified analog substituted DNA molecules with Rh6G dye in 0.1M NaHCO3 buffer. The chemically reactive amino group in AA-dUTP reacts and binds to the succinimidyl ester moiety of the dye Rh6G. Following an overnight reaction with dye under room temperature we again used a PCR clean up kit to remove unreacted dye from the DNA mixture. Then we performed restriction digestion on such dye labeled DNA fragments in-order to create matching overhangs on one end which matches the overhangs on the long DNA which we prepare by digesting plasmids or lambda DNA. We then clean up both dye labeled DNA and longer DNA molecules and ligate labeled fragments to the longer DNA molecules in room temperature overnight.

In practice we create two different restriction overhangs on two ends of the long DNA to which short labeled piece is to be ligated. Since our PCR amplified DNA fragments also have multiple restriction sites on the forward primer region we can create fragments with different overhangs. We create single end labeled long DNA pieces by simply not labeling fragments for one end. Although it is not necessary to ligate pieces to both ends for single end labeling, we found this approach helpful to avoid unwanted long concatamer formation. We also employed a simpler alternative approach which gave both single and double end labeled DNA molecules without having to prepare them separately or have two different restriction sites. We first opened the circular plasmid DNA with a single restriction enzyme and then remove the phosphate group from the both overhangs by treating with alkaline phosphatase and then perform ligation reaction with labeled DNA fragments with matching overhangs. The removal of the phosphate group from the overhangs completely avoids concatamer formation and usually results in both single and double end labeled DNA molecules. However, this approach is only suitable for the shortest DNA chain studied (2.8Kbp). Finally, we used gel electrophoresis (0.75% Agarose gel, TAE buffer, 50 V, 3 hrs) to separate longer end labeled DNA from unreacted fragments. We extract and purify sample using a gel extraction and purification kit (GE Healthcare) following the manufacturers protocol.

For measurements in semidilute regime a small fraction of end-labeled 9 kb DNA was mixed with λ-DNA, and then the solution was slowly evaporated to densities above the overlap concentration of $c^* \sim 25 \pm 5\ \mu g/mL$ for λ-DNA[42,43]. The maximal concentration reached was 3500 $\mu g/mL$ as measured by 260 nm light absorption (using Nanodrop instrument) corresponding to $\sim 140\, c^*$. We note that since the labeled chains are ~ 5.4 times shorter than λ-DNA it might be more proper to discuss solution regimes in terms of the overlap concentration c_l^* of 9 kb DNA which for ideal chain scaling should be $\sqrt{5.4} \sim 2.3$ times lower than that of λ-DNA[44].

Measurements in the dilute regime were carried out at concentration of 2 $\mu g/mL$. All experiments were performed in 10mM Tris, 100 mM NaCl buffer.

4 SFCS Measurements and Discussions

In this section we show experimental implementations of the formalism developed in the Section 2. As we have previously reported the measurements of the overall DNA solution structure[31] and that of individual DNA coils in dilute and semidilute regimes[32], we will not present such data on structure factor measurements with SFCS here. Intead we will focus on SFCS measurements of DNA end-to-end distance distribution and of the dynamics of long DNA chains in dense solutions.

4.1 DNA end-to-end distance distribution

Our motivation for these measurements has been to show that double stranded DNA (dsDNA) behaves as an ideal polymer with only weak interactions between its segments. Theoretical estimations[45,46] and our previous measurements of the structure factor of DNA solutions[31,32] confirm this view.

However, it might be argued that the polymer end-to-end distance distribution $P_{ee}(r_{12})$ is more sensitive to the excluded volume interactions than the whole coil structure factor $S(q)$. Indeed, for the ideal chain $P_{ee}(r_{12})$ has a Gaussian shape with the maximal probability density when the polymer ends are close to each other ($r_{12} = 0$). In contrast, for the real chain $P_{ee} \to 0$ for the close by ends, while $P_{ee}(r_{12})$ maximum shifts to the distances of the order of coil gyration radius[44]. This qualitative difference in the end-to-end distance distribution behaviour between ideal and real chains could allow for more sensitive measurements of DNA nonideality.

The idea of the measurement as outlined in subsection 2.3 is to determine the cross correlation function $G_{12}(r)$ of the two ends by taking the difference of the SFCS functions measured separately from double- and single- end labelled DNA, $G(r)$ and $G_1(r)$, respectively. The Fourier transform of $G_{12}(r)$ then leads to the characteristic function of P_{ee} through the Eq. 13.

In the Fig. 2 we present an example of such a measurement for 2800 bp DNA. The two measured functions $G(r)$ and

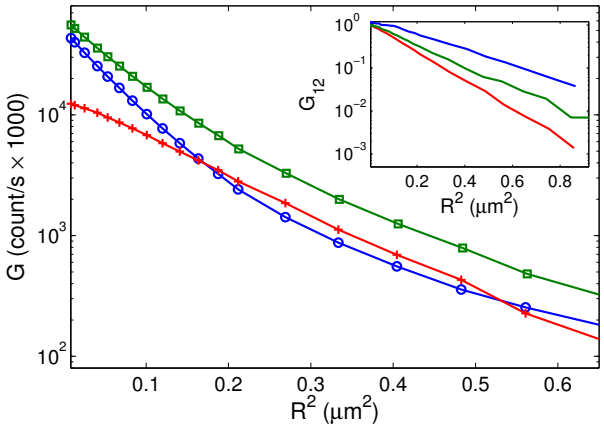

Fig. 2 SFCS measurement of DNA end-to-end distance distribution: $G(R)$ (green squares) and $G_1(R)$ (blue circles) are measured respectively on double- and single-end labeled 2.8 kbp DNA. Their difference $G_{12}(R) = G(R) - G_1(R)$ (red crosses) reflects the cross-correlation in the DNA end positions. Unlike either of $G(R)$ and $G_1(R)$, the cross-correlation $G_{12}(R)$ is Gaussian as expected for an ideal coil. *Inset (top to bottom)*: measured $G_{12}(R)$ for 7.8 kbp, 4.2 kbp and 2.8 kbp DNA respectively.

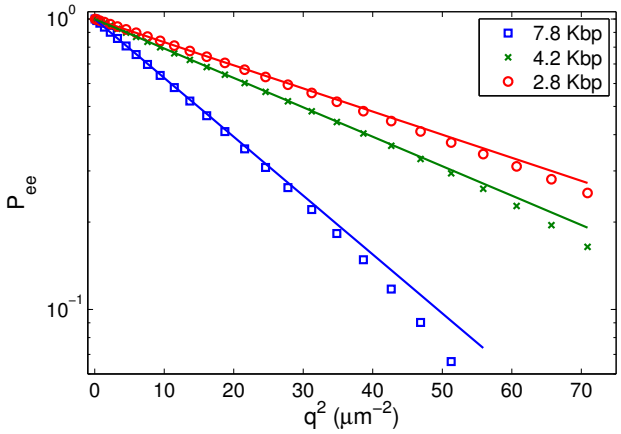

Fig. 3 The characteristic function $P_{ee}(q)$ of the end-to-end distance distribution (normalised as $P_{ee}(0) = 1$) obtained from $G_{12}(R)$ for (*bottom to top*) 7.8 kbp, 4.2 kbp and 2.8 kbp DNA. Solid lines are *not* fits but rather theoretical expectations for ideal chains $P_{ee} = e^{-q^2 L l_p/3}$ with known DNA persistence length of $l_p = 50$ nm and contour lengths L.

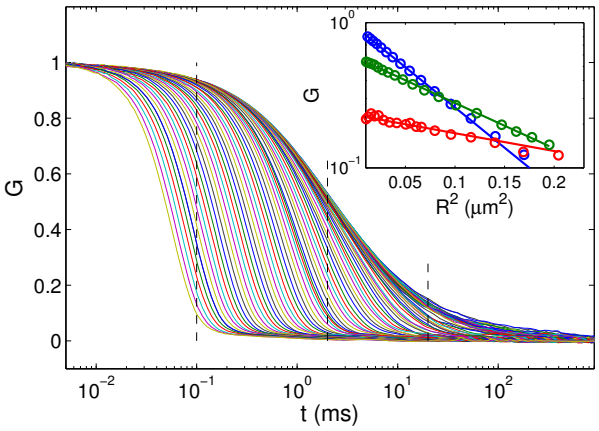

Fig. 4 Example of the application of SFCS technique to measure the segmental dynamics of single end labelled 9 kbp DNA.The SFCS correlations functions (normalised as $G(t \to 0) = 1$) measured at multiple speeds *right to left* from $\sim 1\ \mu m/s$ to $\sim 4400\ \mu m/s$ are analyzed at different time points. *Inset*: extraction of MSD for three time points marked by the vertical dashed lines in the main figure. *Blue, green and red* symbols correspond to 0.1, 2 and 20 ms time points respectively. The line slopes in the figure are related to segmental MSD through the Eq. 14.

$G_1(r)$ are not Gaussian but their difference, $G_{12}(r)$, is Gaussian (the scale in the Fig. 2 is chosen so that Gaussian dependence appears as a straight line). Since the setup OTF is close to the Gaussian, this means that the underlying end-to-end distance distribution is also Gaussian. The measurements of cross-correlations in end positions on longer DNA molecules (inset in Fig. 2) also reveal $G_{12}(r)$ close to Gaussian shape, consistent with the ideal polymer behaviour of DNA.

Respectively, the obtained characteristic functions $P_{ee}(q)$ for all DNA lengths are close to Gaussians up to $q \sim 7\ \mu m^{-1}$, where our measurements become limited by the optical resolution (Fig. 3). For ideal polymers one expects $P_{ee}(q) \propto e^{-q^2\langle r_{12}^2\rangle/6}$ where for the wormlike chain $\langle r_{12}^2\rangle = 2Ll_p$ with L and l_p being the DNA contour and persistence lengths respectively. The solid lines in the Fig. 3 are *not* fits: they are plotted for $\langle r_{12}^2\rangle = 0.095$, 0.14 and 0.27 μm^2 obtained using known DNA $l_p = 50$ nm and DNA contour lengths of $0.95\mu m$, 1.4 μm, 2.6 μm for 2800, 4200, 7800 bp DNA respectively. The theoretical predictions for the ideal chains are remarkably close to the measured $P_{ee}(q)$ supporting the notion of DNA ideal coil behaviour.

This method of measuring end-to-end distance distributions has its natural limits: for a very long polymer its two ends will only rarely simultaneously enter the sampling volume and therefore the difference between $G(R)$ and $G_1(R)$ will be small and buried in statistical noise. On the other end, the method is limited by the optical resolution, so it will not be useful for very short polymers with the end-to-end distance much smaller than w_{xy}.

4.2 DNA dynamics in dense solutions

Static FCS has been successfully applied to measure segmental MSD of DNA in dilute DNA solutions[40,41,47–50]. We demonstrate here that in semi-dilute solutions, where different DNA coils overlap and interpenetrate, static FCS gives erroneous results because of dye photobleaching, yet scanning FCS produces reliable data.

Single-end labeled 9 kb DNA were prepared either in dilute regime or mixed with dense solutions of unlabelled λ-DNA to reach semi-dilute conditions. Then as described in subsection 2.4 a series of independent SFCS measurements were performed at different speeds $\{V_j\}$. As a result, for each sample we obtain a set of correlation curves presented in Fig. 4. At low speeds the correlation curves decay over 3 decades in time reflecting a wide distribution of characteristic time scales in the system. As V_j increases and, respectively, the beam passage time $\tau_V = w_{xy}/V_j$ decreases, more contributions from slow processes with the characteristic times longer than τ_V drop out of the correlation functions, and the latter exhibit progressively faster decay.

Taking values from the curves for the same particular delay time t_i (vertical dashed lines in Fig. 4), we obtain a set of correlation values $G(R_j, t_i)$, with $R_j = V_j t_i$.

As expected from Eq. 14 $G(R_j, t_i)$ are Gaussian functions of displacement R_j with slower decay for larger times t_i (inset in Fig. 4). Provided w_{xy} is calibrated, the segmental MSD $\langle \Delta r^2(t)\rangle$ can be determined for each particular time t_i. Performing this procedure for every available time point, we recover the temporal dependence of the segmental MSD in a wide time window (Fig. 5). Notice, that this method gives an absolute value of $\langle \Delta r^2(t)\rangle$, while the static FCS generally gives only its ratio to w_{xy}^2. Static FCS measurement lacks intrinsic length units, which for SFCS are provided by the speed. Otherwise, for an absolute measurement the setup OTF could be calibrated or, e.g. double-focus FCS modification implemented.[51]

In dilute solutions, the results obtained by SFCS and those obtained by static FCS using Eq. 15 are mutually consistent (Fig. 5, a green line and circles). However, in dense semi-dilute solutions the static FCS approach fails: for concentrations of $\sim 140c^*$ ($\sim 60c_l^*$) the dynamics as extracted from static FCS data is only marginally slower than that in dilute solutions (Fig. 5 red line). The effect of photobleaching is reflected only in the reduced correlation function amplitude (i.e. a smaller effective fluorophore brightness Q), which does not enter the MSD calculations directly. Yet, the scanning FCS approach does reveal the significant slowing down of the DNA segmental dynamics in dense semi-dilute DNA solutions

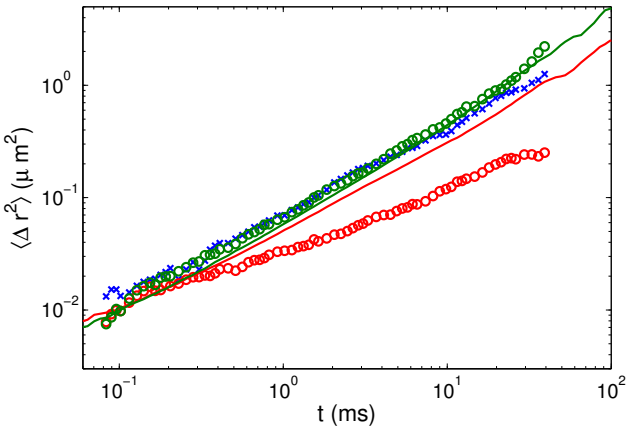

Fig. 5 SFCS measurements of segmental MSD. In dilute solutions static (green line) and scanning (green circles) FCS results are consistent. yet they disagree significantly at high DNA concentration of $c = 140c^*$ (red line and circles for static and scanning FCS respectively). In dense solutions static FCS measurements are unreliable because of fluorophore photobleaching. At moderate concentrations of $\sim 17c^*$ in the semidilute regime, the dynamics measured by scanning FCS (blue crosses) is very close to that of dilute solutions revealing only weak entanglements in these conditions.

(Fig. 5 red circles).

Remarkably, for moderate DNA concentrations of $\sim 415\ \mu g/mL$ that are still deep inside semi-dilute regime ($\sim 17c^*$ or $\sim 7c_l^*$), we do not see any significant change in the DNA segmental dynamics as compared to the measurements in dilute solutions (at $\sim 2\mu g/mL$): the MSD data for these two concentrations are indistinguishable except for long time lags $t > 5ms$ (blue crosses). This means that even though chains overlap and interpenetrate significantly, they are essentially not entangled within the temporal range of < 5 ms and MSD range $< 0.4\ \mu$m^2. This finding is consistent with semiflexible nature of DNA: there is ample free volume within each chain, so that the excluded volume interactions are weak and the segmental dynamics is essentially uninhibited.

While here we used specific labelling that measure segmental MSD kinetics, other labelling strategies can be used with SFCS to highlight different dynamic modes: e.g. homogeneous tagging of the chains should reveal the cooperative diffusion of polymer chains due to the fluctuations in monomer density.

We note finally, that with some minor modifications in the formalism our SFCS approach might be instrumental in studying more complex soft matter systems where deducing the system dynamics from standard FCS experiments is not easy (e.g. such as in[52]). Having an additional experimental parameter - the speed of scanning - one could e.g. conceivably distinguish between two-component diffusion and subdiffusion phenomena, that sometimes are difficult to separate in a standard FCS.

5 Conclusions

Here we presented the theoretical formalism and an experimental realisation of a novel approach to measure structure and dynamics of soft matter systems. The combination of specific fluorescence labelling with scanning FCS allows us to measure the structure factor of whole polymer solutions, the structure factor of individual chains, polymer end-to-end distance distribution and segmental MSD kinetics in dilute and in dense solutions.

We demonstrated the application of this method by measuring the end-to-end distance distribution and the segmental dynamics of DNA molecules. The end-to-end distance distribution is Gaussian with the characteristic mean square distance obeying $\langle r_{12}^2 \rangle = 2Ll_p$ as predicted by the ideal worm-like chain with $l_p = 50$ nm. The segmental dynamics results obtained by static and scanning FCS in dilute solutions are mutually consistent. However, in semidilute solutions scanning FCS produces more reliable data by removing molecules from the sampling volume before they photobleach. Surprisingly, up to rather high concentrations of $\sim 17c^*$ ($\sim 7c_l^*$), deep in the semidilute regime, the segmental dynamics does not exhibit any appreciable polymer entanglements.

These findings together with our previously published results on the structure of DNA coils and solutions[31,32] are consistent with the general view of the weakness of excluded volume interactions in semiflexible polymers[45,46].

The formalism presented here can be readily adapted for a scanning counterpart of dual-color FCS[53]: one can use this approach to study correlations in positions and motions of differently labeled objects. SFCS is also fully compatible with Stimulated Emission Depletion (STED) optics[54] and its further incorporation into our approach would allow one to assess soft matter system static and dynamic structure factors at subdiffraction resolutions.

*

References

1 D. Magde, E. Elson and W. Webb, *Phys. Rev. Lett.*, 1972, **29**, 705–708.
2 D. Magde, E. L. Elson and W. W. Webb, *Biopolymers*, 1974, **13**, 29–61.
3 E. L. Elson and D. Magde, *Biopolymers*, 1974, **13(1)**, 1–27.
4 R. Rigler, U. Mets, J. Widengren and P. Kask, *Europ. J. Biophys.*, 1993, **22**, 169–175.
5 N. L. Thompson, A. M. Lieto and N. W. Allen, *Curr. Opin. Struct. Biol.*, 2002, **12**, 634–641.
6 E. Elson, *Biophys J.*, 2011, **101(12)**, 2855–70.

* This work was supported by Israel Science Foundation Grants No. 984/09 and 1912/14 and German-Israeli Foundation grant No. 972-146.14/2007. M.N. was supported by EC FP7 Marie Curie program (No. 215148).

7 S. T. Hess, S. Huang, A. A. Heikal and W. W. Webb, *Biochemistry.*, 2002, **41(3)**, 697–705.
8 O. Krichevsky and G. Bonnet, *Rep. Prog. Phys.*, 2002, **65**, 251297.
9 J. Ries and P. Schwille, *Bioessays.*, 2012, **34(5)**, 361–8.
10 G. Bonnet, O. Krichevsky and A. Libchaber, *Proc. Natl. Acad. Sci.*, 1998, **95(15)**, 8602–8606.
11 R. B. Yirdaw and H. S. Mchaourab, *Biophys. J.*, 2012, **103**, 1525–1536.
12 E. Sherman and G. Haran, *Chemphyschem.*, 2011, **12(3)**, 696–703.
13 A. Schenk, S. Ivanchenko, C. Rocker, J. Wiedenmann and G. Nienhaus, *Biophys J.*, 2004, **86(1 Pt 1)**, 384–394.
14 A. M. Lieto, R. C. Cush and N. L. Thompson, *Biophys J.*, 2003, **85(5)**, 3294–3302.
15 U. Kettling, A. Koltermann, P. Schwille and M. Eigen, *Proc. Natl Acad. Sci. USA*, 1998, **95**, 1416–1420.
16 M. Weissman, H. Schindler and G. Feher, *Proc. Natl Acad. Sci. USA*, 1976, **73**, 2776–2780.
17 D. Magde, W. W. Webb and E. L. Elson, *Biopolymers*, 1978, **17**, 361–376.
18 N. Petersen, P. Hddelius, P. Wiseman, O. Seger and K. Magnusson, *Biophys J*, 1993, **65**, 1135 – 1146.
19 D. Kolin and P. Wiseman, *Cell Biochemistry and Biophysics*, 2007, **49**, 141–164.
20 B. Hebert, S. Costantino and P. W. Wiseman, *Biophysical Journal*, 2005, **88**, 3601 – 3614.
21 P. W. Wiseman, *Cold Spring Harbor Protocols*, 2015, **2015**, 336–348.
22 N. O. Petersen, *Biophysical Journal*, 1986, **49**, 809–815.
23 N. O. Petersen, D. C. Johnson and M. J. Schlesinger, *Biophysical Journal*, 1986, **49**, 817–820.
24 M. A. Digman, P. Sengupta, P. W. Wiseman, C. M. Brown, A. R. Horwitz and E. Gratton, *Biophysical Journal*, 2005, **89**, 1317–1327.
25 Z. Petrasek, J. Ries and P. Schwille, *Methods Enzymol.*, 2010, **472**, 317–343.
26 J. P. Skinner, Y. Chen and J. D. Muller, *Biophysical Journal*, 2005, **89**, 1288–1301.
27 D. Koppel, F. Morgan, A. Cowan and J. Carson, *Biophysical Journal*, 1994, **66**, 502 – 507.
28 Q. Ruan, M. A. Cheng, M. Levi, E. Gratton and W. W. Mantulin, *Biophysical Journal*, 2004, **87**, 1260 – 1267.
29 Z. Petrasek and P. Schwille, *Biophysical Journal*, 2008, **94**, 1437–1448.
30 Z. Petrasek, S. Derenko and P. Schwille, *Opt Express.*, 2011, **19(25)**, 25006–21.
31 E. Shafran, A. Yaniv and O. Krichevsky, *Phys. Rev. Lett.*, 2010, **104**, 128101.
32 M. Nepal, A. Yaniv, E. Safran and O. Krichevsky, *Phys. Rev. Lett.*, 2013, **110**, 058102.
33 B. J. Berne and R. Pecora, *Dynamic Light Scattering*, Wiley, New York, 1976.
34 J. P. Hansen and J. R. McDonald, *Theory of Simple Liquids*, Academic, New York, 2005.
35 F. Höfling, K. U. Bamberg and T. Franosch, *Soft Matter*, 2011, **7**, 1358–1363.
36 F. Höfling and T. Franosch, *Rep. Prog. Phys.*, 2013, **76**, 046602.
37 M. Daoud, J. P. Cotton, B. Farnoux, G. Jannink, G. Sarma, H. Benoit, R. Duplessix, C. Picot and P.-G. deGennes, *Macromolecules*, 1975, **8**, 804–818.
38 B. Farnoux, F. Boue, J. P. Cotton, M. Daoud, G. Jannink, M. Nierlich and P.-G. deGennes, *J. Phys. (Paris)*, 1978, **39**, 77.
39 L. H. Sperling, *Polym. Eng. Sci.*, 1984, **24**, 1.
40 A. Bernheim-Groswasser, R. Shusterman and O. Krichevsky, *J. Chem. Phys.*, 2006, **125**, 084903.
41 R. Shusterman, T. Gavrinyov and O. Krichevsky, *Phys. Rev. Lett.*, 2008, **100**, 098102.
42 R. Verma, J. C. Crocker, T. C. Lubensky and A. G. Yodh, *Phys. Rev. Lett.*, 1998, **81**, 4004–7.
43 N. Pernodet and B. Tinland, *Biopolymers*, 1997, **42**, 471.
44 P.-G. de Gennes, *Scaling Concepts in Polymer Physics*, Cornell University Press, Ithaca and London, 1993.
45 D. W. Schaefer, J. F. Joanny and P. Pincus, *Macromol.*, 1980, **13**, 1280–1289.
46 J. F. Marko and E. D. Siggia, *Phys. Rev. E*, 1995, **52**, 2912–2938.
47 D. Lumma, S. Keller, T. Vilgis and J. O. Rädler, *Phys. Rev. Lett.*, 2003, **90**, 218301.
48 R. Shusterman, S. Alon, T. Gavrinyov and O. Krichevsky, *Phys. Rev. Lett.*, 2004, **92**, 048303.
49 E. P. Petrov, T. Ohrt, R. G. Winkler and P. Schwille, *Phys. Rev. Lett.*, 2006, **97**, 258101.
50 T. Kalkbrenner, A. Arnold and S. J. Tans, *Biophys J.*, 2009, **96**, 4951.
51 T. Dertinger, V. Pacheco, I. von der Hocht, R. Hartmann, I. Gregor and J. Enderlein, *Chemphyschem*, 2007, **8**, 433–43.
52 A. Vagias, R. Raccis, K. Koynov, U. Jonas, H.-J. Butt, G. Fytas, P. Košovan, O. Lenz and C. Holm, *Phys. Rev. Lett.*, 2013, **111**, 088301.
53 P. Schwille, F. J. Meyer-Almes and R. Rigler, *Biophys. J.*, 1997, **72**, 1878–86.
54 A. Honigmann, V. Mueller, H. Ta, A. Schoenle, E. Sezgin, S. W. Hell and C. Eggeling, *Nat. Commun.*, 2014, **5**, 5412.

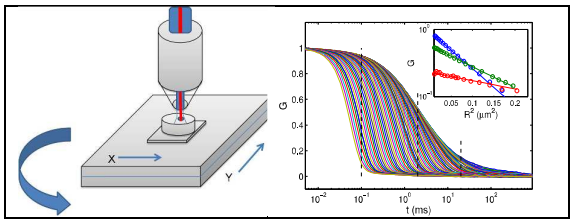

Scanning Fluorescence Correlation spectroscopy in combination with specific fluorescent labeling is used to measure different static and dynamic properties of a soft matter system.